Caspase-3 triggers early synaptic dysfunction in a mouse model of Alzheimer's Disease

Marcello D'Amelio, Virve Cavallucci, Silvia Middei, Cristina Marchetti, Simone Pacioni, Alberto Ferri, Adamo Diamantini, Daniela De Zio, Paolo Carrara, Luca Battistini, Sandra Moreno, Martine Ammassari-Teule, Hélène Marie and Francesco Cecconi

Supplementary Informations:

Supplementary Figures 1-23

Nature Neuroscience: doi:10.1038/nn.2709

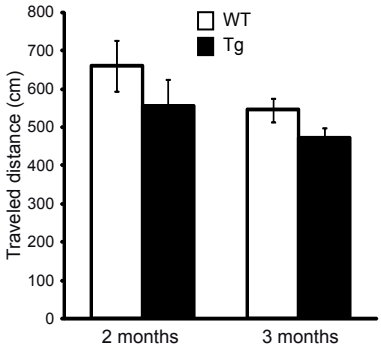

Supplementary Figure 1. Baseline activity in CFC.

Distance traveled (cm) by 2- and 3-month-old wild-type (WT) and Tg2576 (Tg) mice during the 2-minutes habituation in CFC training phase. Values are averaged per group and expressed as mean ± s.e.m.

Nature Neuroscience: doi:10.1038/nn.2709

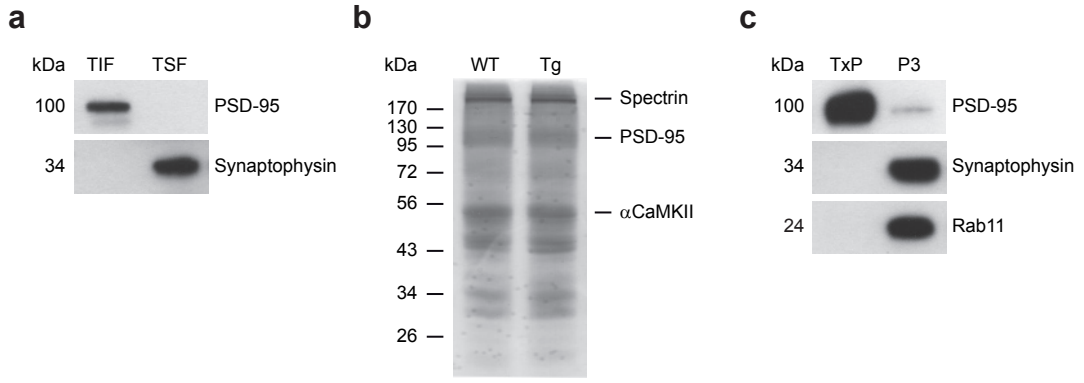

Supplementary Figure 2. Characterization of PSD preparation and synaptic fractionation.

a, Immunoblot analysis of PSD-95 and synaptophysin demonstrating the purity of the PSD preparation. Representative immunoblots of the PSD fraction (Triton Insoluble Fraction, TIF) and of the fraction containing synaptic cytosolic components (Triton Soluble Fraction, TSF) are shown. **b,** PSD protein preparations (15 μg protein) from wild-type (WT) and Tg2576 (Tg) individuals were separated by SDS-PAGE and stained with Coomassie brilliant blue. No major differences are seen at this level of resolution. **c,** Immunoblot analysis of PSD-95, synaptophysin and Rab11 demonstrating the purity of the synaptic fractionation. Representative immunoblots of the PSD-enriched fraction (TxP) and of the microsomal-enriched fraction (P3) are shown.

Nature Neuroscience: doi:10.1038/nn.2709

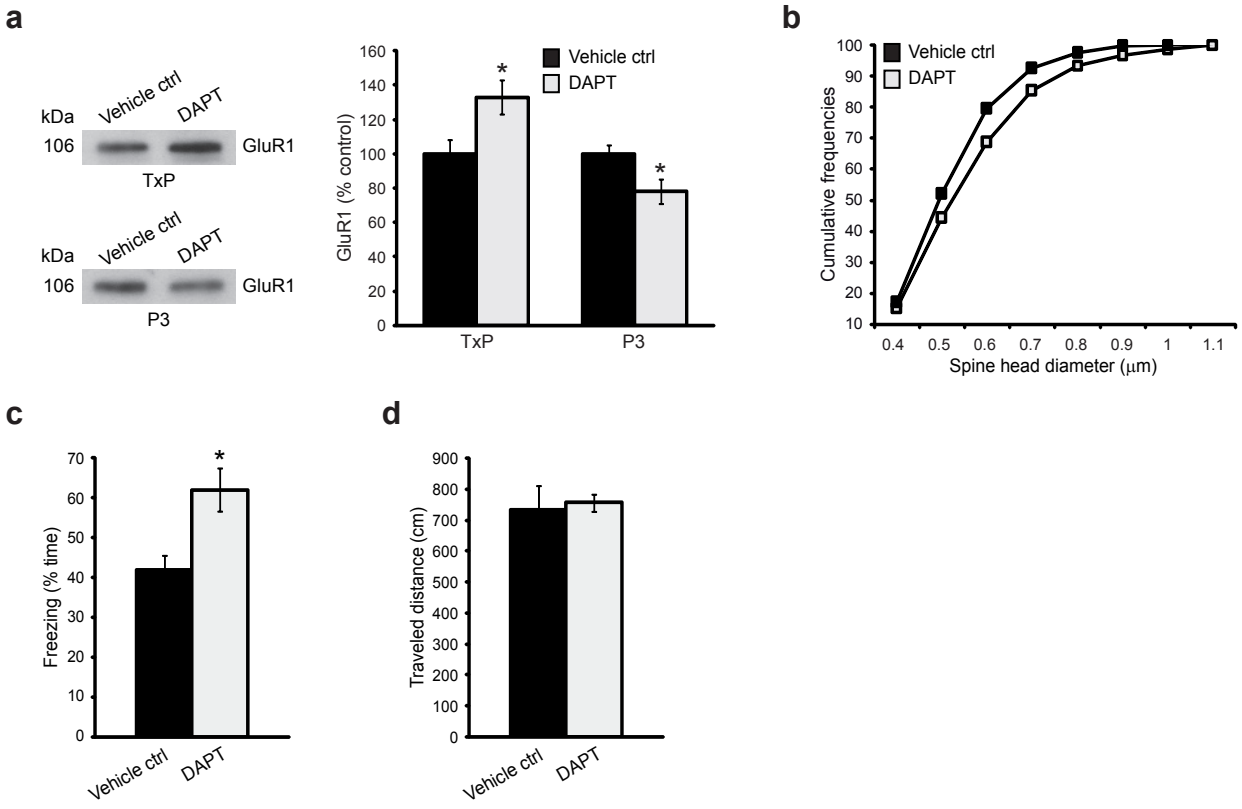

Supplementary Figure 3. Inhibiting APP proteolysis, *in vivo*, leads to GluR1 redistribution and rescues spine head size and memory function in Tg2576 mice.

a, The γ-secretase inhibitor (DAPT) and vehicle control (DMSO) were administered via *intra*-hippocampal injection into 3-month-old Tg2576 mice. 15 hrs after injection synaptic fractionation was performed. Representative GluR1 immunoblots and densitometric quantification of changes in gray values expressed as mean ± s.d. (control is indicated as 100%). **P*=0.037 (*N*=4 mice). **b,** Graph shows cumulative frequencies of spine head diameters in apical dendrites after injection of DAPT or vehicle. *P*=0.0003 (*N*=4 mice, *n*=1000 spine per group). **c,** Percentage of freezing time during CFC test in vehicle- and DAPT-treated Tg2576 mice. Data are expressed as mean ± s.e.m. **P*=0.036 (*N*=5 vehicle-injected mice, *N*=6 DAPT-injected mice). **d,** Distance traveled (cm) during the 2-minutes habituation in CFC training phase by Tg2576 mice injected with DAPT or vehicle. Values are averaged per group and expressed as mean ± s.e.m.

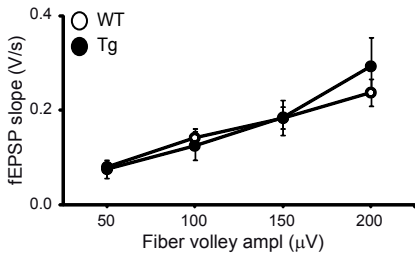

Supplementary Figure 4. Input-output relationships.

Input-output relationships (fEPSP slopes vs. increasing afferent fiber volley amplitudes) in 3-month-old wild-type (WT, *n*=20 slices) and Tg2576 (Tg, *n*=14) mice.

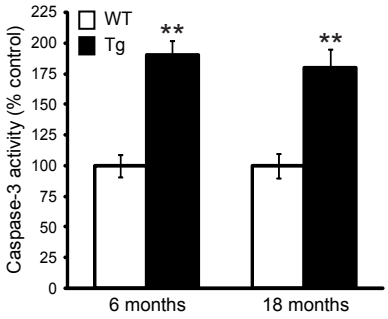

Supplementary Figure 5. Caspase-3 activity in the hippocampus of 6- and 18-month old mice. Caspase-3 activity was revealed by a fluorimetric assay in hippocampal synaptosomes from wild-type (WT) and Tg2576 (Tg) mice. The histogram shows the caspase-3 activity mean ± s.d. (wild-type is indicated as 100%). ***P*=0.004 (*N*=4 mice for each age and genotype).

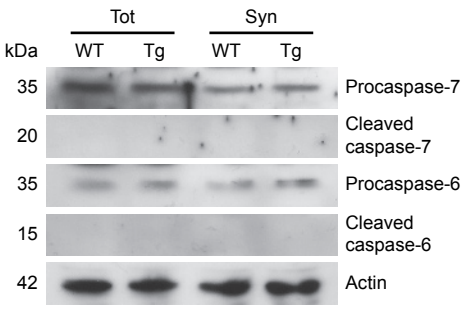

Supplementary Figure 6. Caspase-6 and -7 are not active in the hippocampus.

Representative immunoblots showing that caspase-6 and -7 are not cleaved both in total homogenates (Tot) and in synaptosome (Syn) preparations from hippocampus of 3-month-old wild-type (WT) and Tg2576 (Tg) mice.

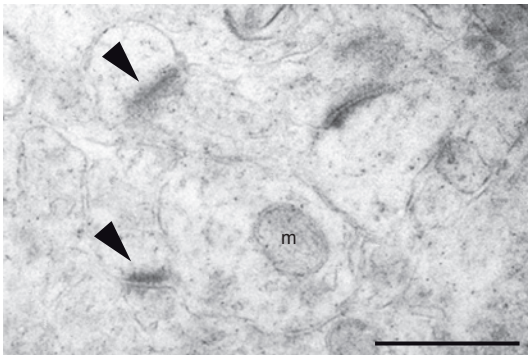

Supplementary Figure 7. Electron microscopy of unstained section of CA1 hippocampus region.

Unstained control of pre-embedding immunohistochemistry on ultrathin sections. The arrowheads indicate dendritic spines. Scale bar, 0.5 μm. m: mitochondrion.

Nature Neuroscience: doi:10.1038/nn.2709

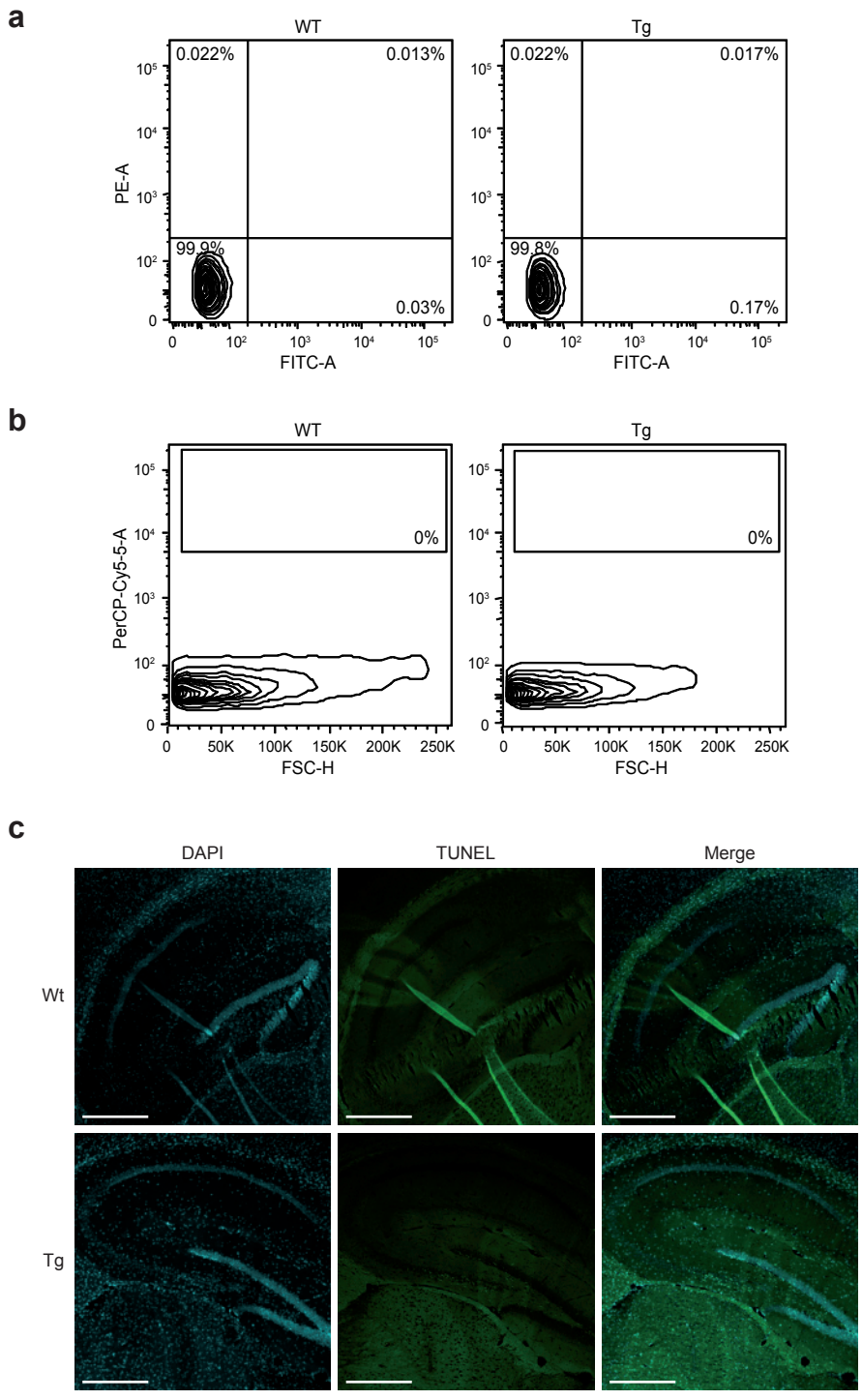

Supplementary Figure 8. Flow cytometry analysis of unstained controls and TUNEL assay.

a, Distribution of unstained synaptosomes preparation from wild-type (WT) and Tg2576 (Tg) hippocampi. **b,** Distribution of unstained nuclei preparation. **c,** Representative images of the hippocampus of 3-month-old wild-type (WT) and Tg2576 (Tg) brain sections analyzed by TUNEL assay. Scale bar, 50 μm.

Nature Neuroscience: doi:10.1038/nn.2709

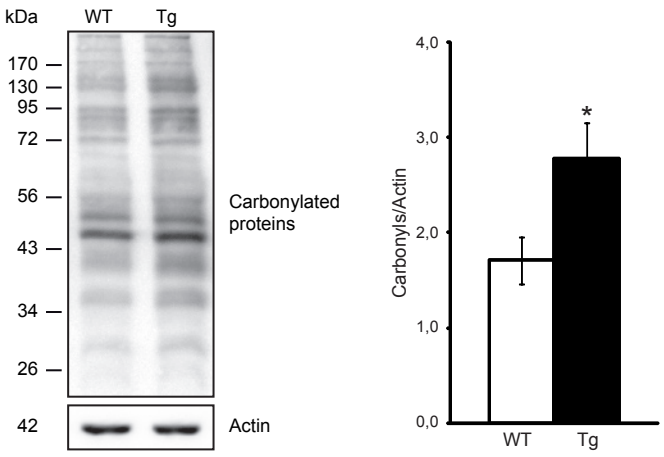

Supplementary Figure 9. Immunoblotting analysis of oxidative damage in hippocampus.

Representative immunoblot showing oxidative damage, revealed by carbonylation of proteins prepared from the hippocampus of 3-month-old wild-type (WT) and Tg2576 (Tg) mice. Graph shows the densitometric analysis of each lane (actin was used as a loading control). Data are expressed as mean ± s.d. **P*=0.039 (*N*=7 mice for each genotype).

Nature Neuroscience: doi:10.1038/nn.2709

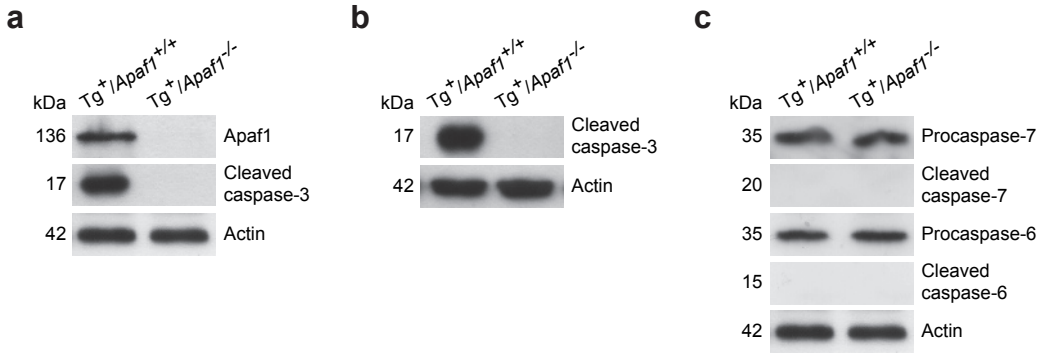

Supplementary Figure 10. The apoptosome pathway is the main route of caspase-3 activation in Tg2576-derived primary neurons.

a, Total cell lysates from Tg2576-derived primary hippocampal cultured neurons in the presence or absence of the apoptosome protein Apaf1 ($Tg^{+}/Apaf1^{+/+}$ or $Tg^{+}/Apaf1^{-/-}$, respectively) were blotted and probed for caspase-3 processing. **b,** Synaptosome preparations from $Tg^{+}/Apaf1^{+/+}$ and $Tg^{+}/Apaf1^{-/-}$ primary hippocampal cultured neurons were blotted and probed for caspase-3 processing. **c,** Total cell lysates from $Tg^{+}/Apaf1^{+/+}$ and $Tg^{+}/Apaf1^{-/-}$ were blotted and probed for processing of caspase-7, and -6. No caspases analyzed are cleaved, both in $Tg^{+}/Apaf1^{+/+}$ and $Tg^{+}/Apaf1^{-/-}$ neurons.

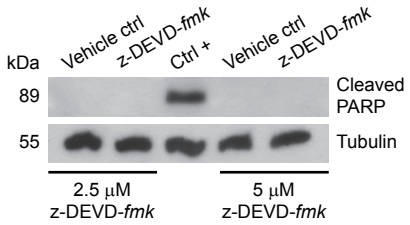

Supplementary Figure 11. Slicing conditions used do not induce caspase-3 dependent apoptosis.

After 2 hrs of z-DEVD-*fmk* incubation (2,5 or 5 μM), protein extracts from each sample were analyzed by immunoblotting with an anti-cleaved PARP antibody. The analysis shows that in both experimental conditions PARP is not processed. Ctrl +: extracts from slices exposed to 20 μM staurosporine for 2 hrs are used as a positive control of PARP cleavage.

Nature Neuroscience: doi:10.1038/nn.2709

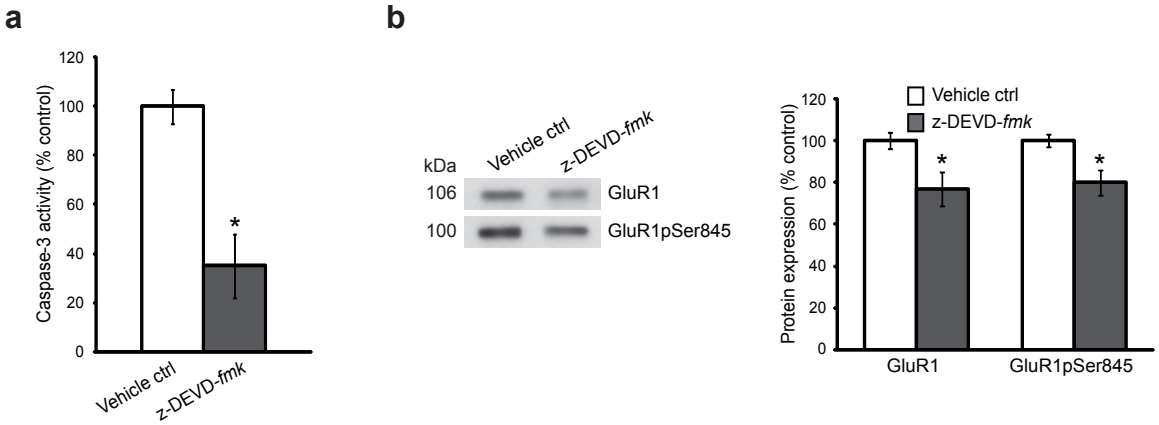

Supplementary Figure 12. Inhibiting caspase-3 activity in wild-type hippocampal slices causes an inverse effect on GluR1 surface expression.

a, Hippocampal slices taken from 3-month-old wild-type mice were incubated in the presence of 5 μM z-DEVD-*fmk* or vehicle control for 2 hrs. Caspase-3 activity was analyzed by fluorimetric method and the data are expressed as mean ± s.d. (control is indicated as 100%). **P*=0.021 (*N*=4 mice). **b,** Representative immunoblots and densitometric analysis of GluR1 and GluR1pSer845 in PSD proteins extracted from wild-type hippocampal slices incubated in the presence of 5 μM z-DEVD-*fmk* or vehicle control for 2 hrs. The data shown in the graph are expressed as mean ± s.d. (control is indicated as 100%). **P*=0.041 (*N*=4).

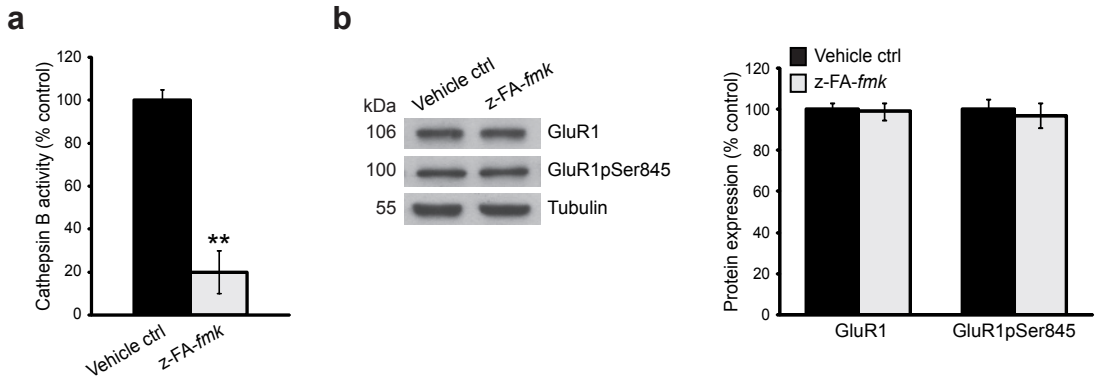

Supplementary Figure 13. z-FA-*fmk* treatment of Tg2576 hippocampal slices does not influence GluR1 phosphorylation.

a, Hippocampal slices taken from 3-month-old Tg2576 mice were incubated in the presence of 5 μM z-FA-*fmk* or vehicle control (DMSO) for 2 hrs. Cathepsin B activity was analyzed by fluorimetric method; data are expressed as mean ± s.d. (control is indicated as 100%). ***P*=0.008 (*N*=3 mice). **b,** Representative immunoblots and densitometric analysis of GluR1 and GluR1pSer845 in total protein extract from slices incubated with 5 μM z-FA-*fmk* or with vehicle control for 2 hrs. The data shown in the graph are expressed as mean ± s.d. (control is indicated as 100%). (*N*=3).

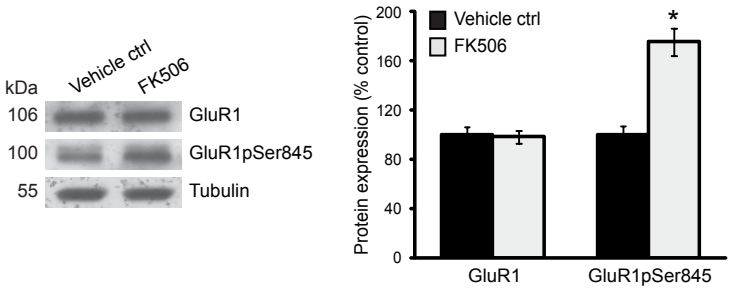

Supplementary Figure 14. FK506 treatment of Tg2576 hippocampal slices increases GluR1 phosphorylation.

Representative immunoblots and densitometric analysis of GluR1 and GluR1pSer845 in total protein extract from slices incubated with 10 μM FK506 or with vehicle control (DMSO) for 2 hrs. The data shown in the graph are expressed as mean ± s.d. (control is indicated as 100%). **P*=0.022 (*N*=4).

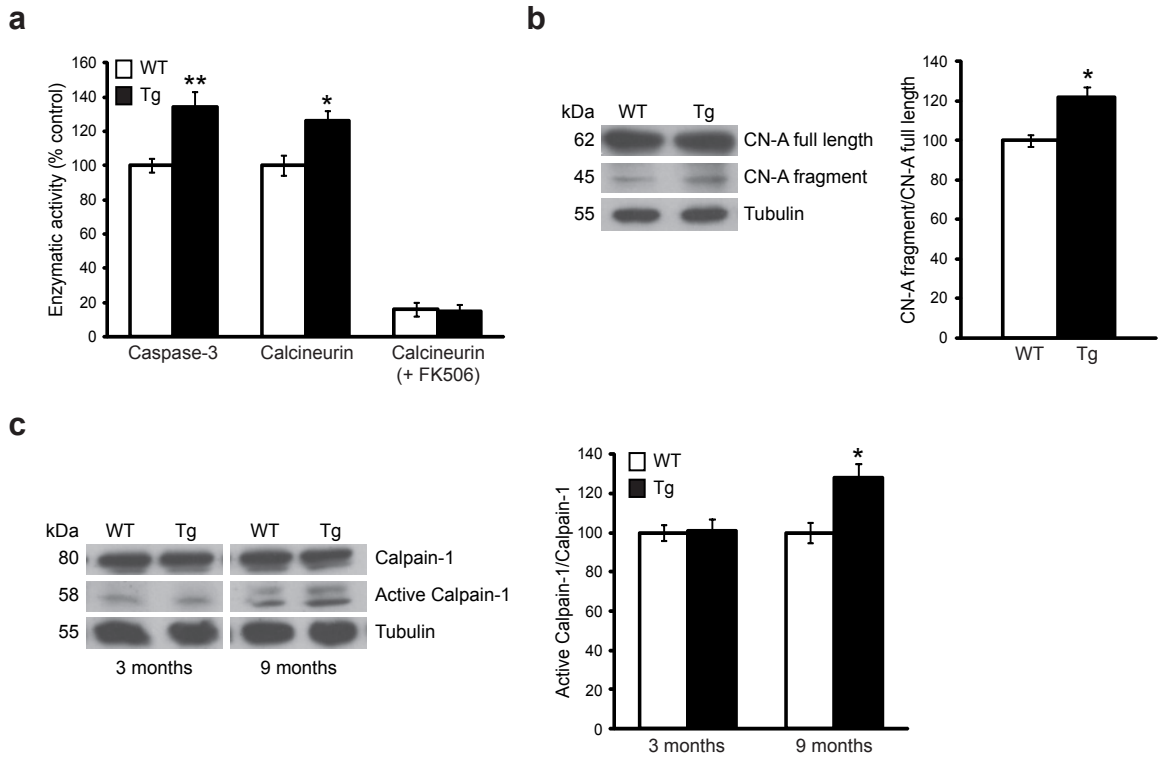

Supplementary Figure 15. Calcineurin but not calpain-1 is increased in 3-month-old Tg2576 hippocampus *in vivo*.

a, Caspase-3 and calcineurin activities were analyzed in hippocampus of 3-month-old wild-type (WT) and Tg2576 (Tg) mice. As control of calcineurin activity, FK506 was added to protein extracts (+ FK506). Data are expressed as mean ± s.d. (control is indicated as 100%). ***P*=0.003, **P*=0.021 (*N*=6 mice from each genotype). **b,** Representative immunoblot and densitometric analysis of CN-A full length and its N-terminal fragment in total protein extract from hippocampus of 3-month-old wild-type and Tg2576 mice. The data shown in the graph are expressed as mean ± s.d. (control is indicated as 100%). **P*=0.029 (*N*=4). **c,** Representative immunoblot and densitometric analysis of latent and active calpain-1 in total protein extract from hippocampus of 3- and 9-month-old wild-type and Tg2576 mice. The data shown in the graph are expressed as mean ± s.d. (control is indicated as 100%). **P*=0.032 (*N*=4).

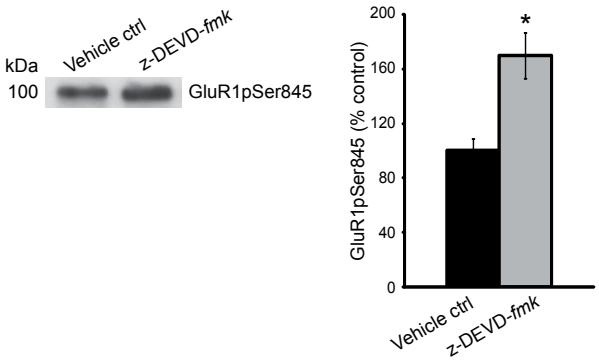

Supplementary Figure 16. Inhibiting caspase-3 activity - *in vivo* - leads to increase of GluR1pSer845 at the PSD in Tg2576 mice.

The caspase-3 inhibitor (z-DEVD-*fmk*) or vehicle control (DMSO) were administered via *intra*-hippocampal injection into 3-month-old Tg2576 mice. 15 hrs after injection PSD preparation was performed. Representative GluR1pSer845 immunoblot of hippocampal PSD proteins. Graph shows densitometric quantification of changes in gray values expressed as mean ± s.d. (control is indicated as 100%). **P*=0.032 (*N*=4).

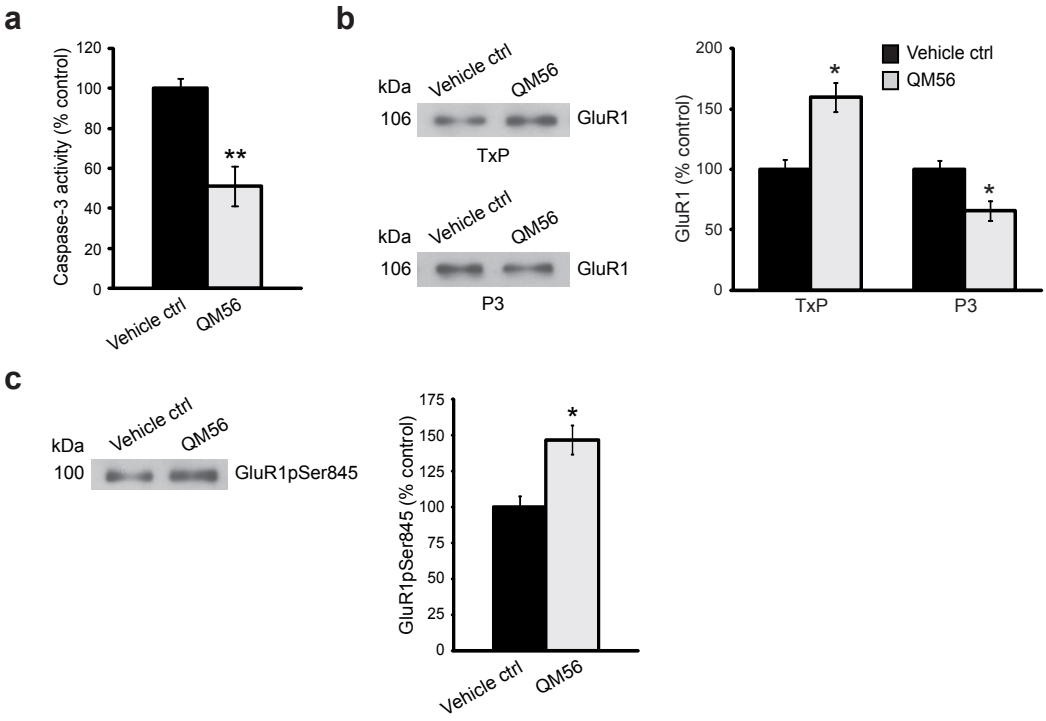

Supplementary Figure 17. Inhibiting apoptosome - *in vivo* - reduces caspase-3 activity, influences GluR1 distribution and leads to increase of GluR1pSer845 at the PSD in Tg2576 mice.

a, 48 hrs after *intra*-hippocampal injection of QM56 or vehicle into 3-month-old Tg2576 mice, caspase-3 activity was analyzed. The data are expressed as mean ± s.d. (control is indicated as 100%). ***P*=0.009 (*N*=4 mice). **b,** Representative immunoblots of hippocampus synaptic fractionation performed 48 hrs after QM56 or vehicle injection and GluR1 densitometric quantification of changes in grey values expressed as mean ± s.d. (control is indicated as 100%). **P*=0.029 (TxP), **P*=0.033 (P3) (*N*=4). TxP, PSD-enriched fraction; P3, microsome-enriched fraction. **c,** Representative GluR1pSer845 immunoblot of hippocampal PSD proteins. Graph shows densitometric quantification of changes in gray values expressed as mean ± s.d. (control is indicated as 100%). **P*=0.030 (*N*=4).

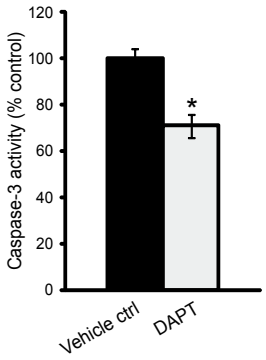

Supplementary Figure 18. Inhibiting APP proteolysis, *in vivo*, reduces caspase-3 activity in Tg2576 mice.

15 hrs after *intra*-hippocampal injection of DAPT or vehicle into 3-month-old Tg2576 mice, caspase-3 activity was analyzed. The data are expressed as mean ± s.d. (control is indicated as 100%). **P*=0.021 (*N*=4 mice).

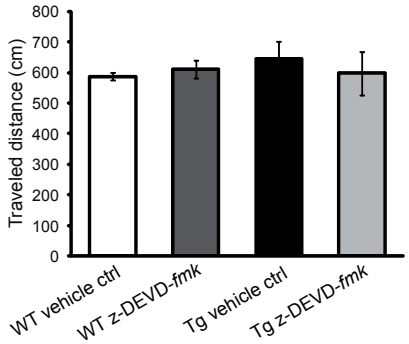

Supplementary Figure 19. Baseline activity in CFC.

Distance traveled (cm) by wild-type (WT) and Tg2576 (Tg) mice treated with z-DEVD-*fmk* or vehicle during the 2-minutes habituation in CFC training phase. Values are averaged per group and expressed as mean ± s.e.m.

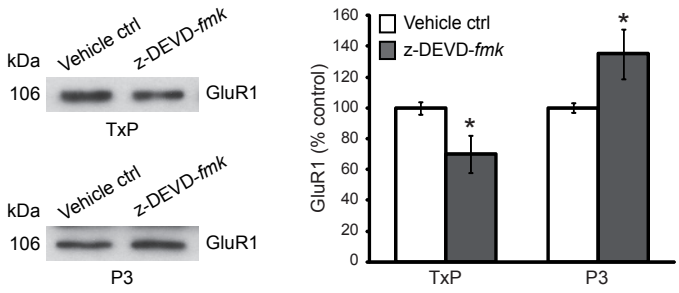

Supplementary Figure 20. Caspase-3 inhibition *in vivo* alters GluR1 distribution in wild-type mice.

15 hrs after *intra*-hippocampal injection of z-DEVD-*fmk* or vehicle into 3-month-old WT mice, hippocampus synaptic fractionation was performed. Representative GluR1 immunoblots and densitometric quantification of changes in grey values expressed as mean ± s.d. (control is indicated as 100%). **P*=0.035 (N=4 mice). TxP, PSD-enriched fraction; P3, microsome-enriched fraction.

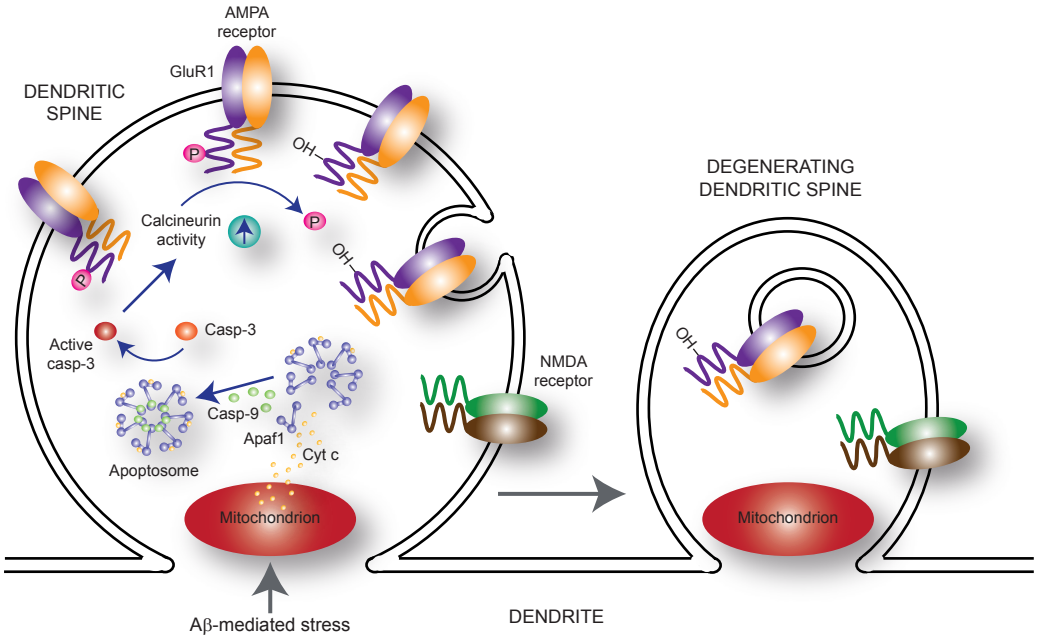

Supplementary Figure 21. Model of the role of caspase-3 in dendritic spine degeneration.

Nature Neuroscience: doi:10.1038/nn.2709

Fig. 2c

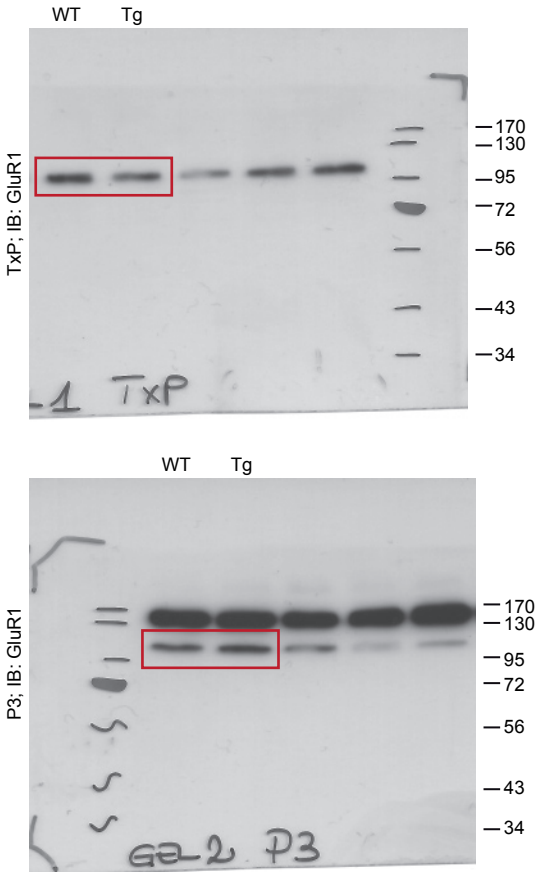

Fig. 4b

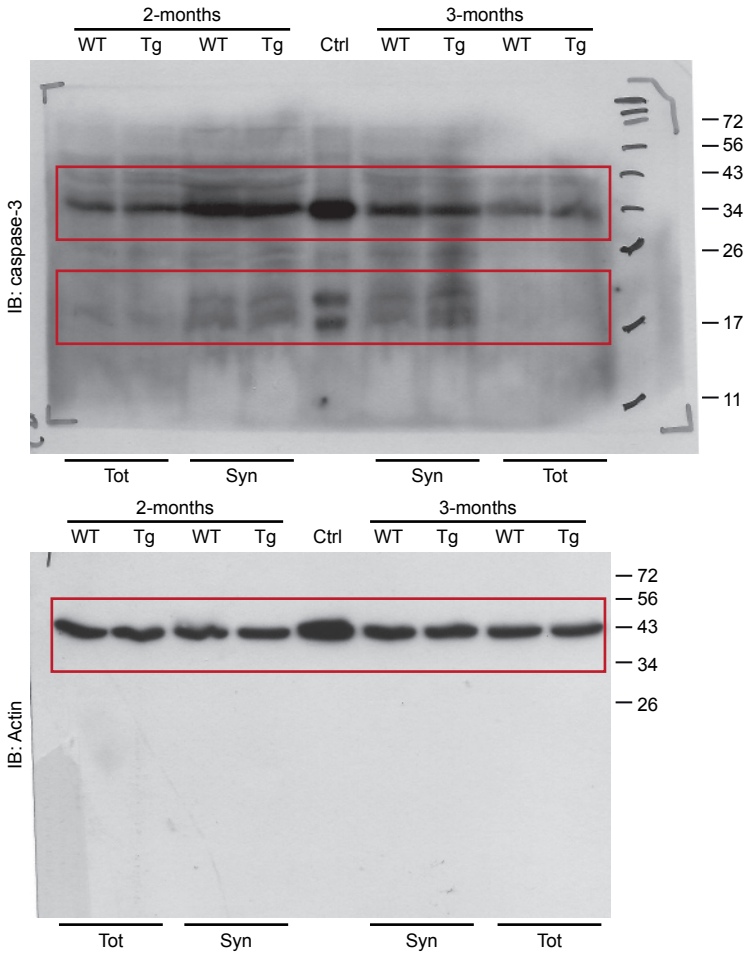

Supplementary Figure 22. Full-length blots for figures in the main text. The cropped areas shown in the main figures are boxed in red. Several membranes were cut to process multiple antibodies per blot, for which full-length blots cannot be shown.

Fig. 5b

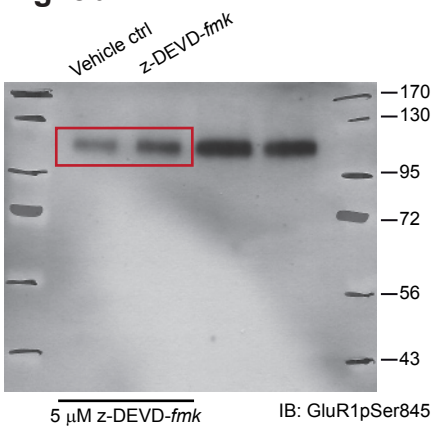

Fig. 5d

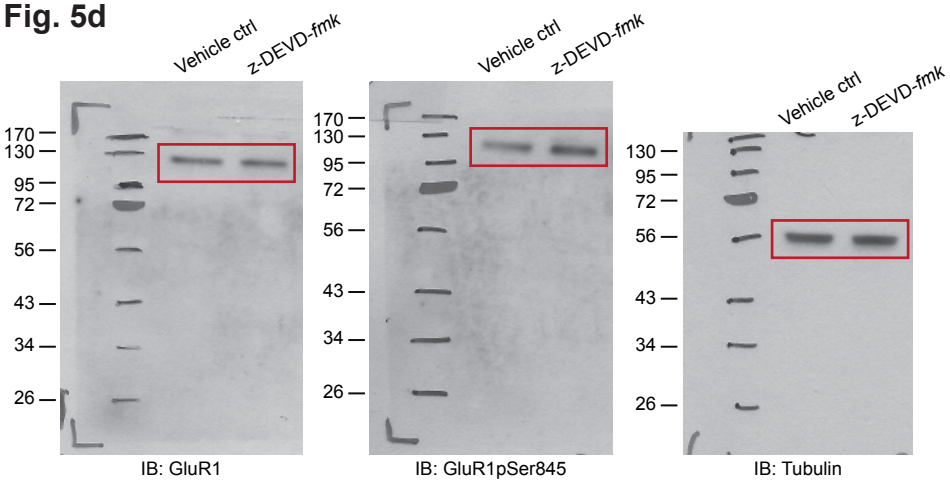

Fig. 7c

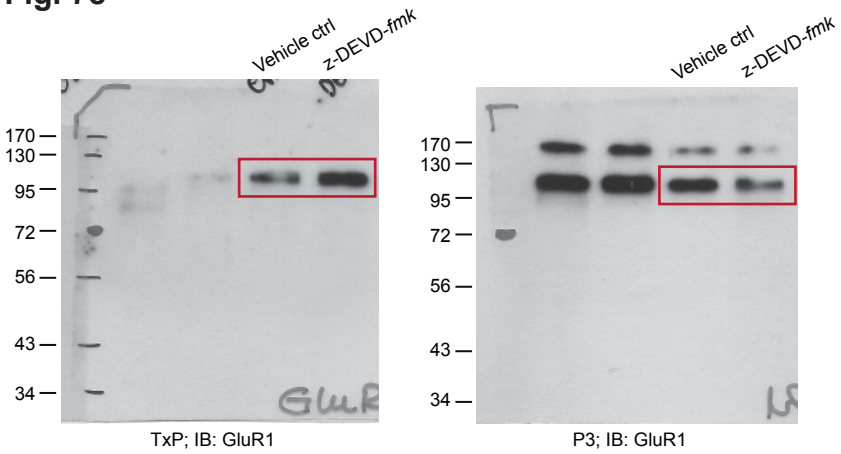

Supplementary Figure 23. Full-length blots for figures in the main text. The cropped areas shown in the main figures are boxed in red. Several membranes were cut to process multiple antibodies per blot, for which full-length blots cannot be shown.